AFRL-AFOSR-VA-TR-2024-0064

Passive Control of Non-Canonical Flows with Anisotropic Porous Materials

FARRUKH ALVI
FLORIDA STATE UNIV TALLAHASSEE
874 TRADITIONS WAY
TALLAHASSEE, FL, 32306 - 0001
US

12/08/2023
Final Technical Report

Air Force Research Laboratory
Air Force Office of Scientific Research
Arlington, Virginia 22203
Air Force Materiel Command

REPORT DOCUMENTATION PAGE

PLEASE DO NOT RETURN YOUR FORM TO THE ABOVE ORGANIZATION.

1. REPORT DATE	2. REPORT TYPE	3. DATES COVERED	
20231208	Final	START DATE 20211001	END DATE 20230814

4. TITLE AND SUBTITLE
Passive Control of Non-Canonical Flows with Anisotropic Porous Materials

5a. CONTRACT NUMBER	5b. GRANT NUMBER	5c. PROGRAM ELEMENT NUMBER
	FA9550-21-1-0286	61102F
5d. PROJECT NUMBER	**5e. TASK NUMBER**	**5f. WORK UNIT NUMBER**

6. AUTHOR(S)
Farrukh Alvi

7. PERFORMING ORGANIZATION NAME(S) AND ADDRESS(ES)
FLORIDA STATE UNIV TALLAHASSEE
874 TRADITIONS WAY
TALLAHASSEE, FL 32306 - 0001
US

8. PERFORMING ORGANIZATION REPORT NUMBER

9. SPONSORING/MONITORING AGENCY NAME(S) AND ADDRESS(ES)	10. SPONSOR/MONITOR'S ACRONYM(S)	11. SPONSOR/MONITOR'S REPORT NUMBER(S)
Air Force Office of Scientific Research 875 N. Randolph St. Room 3112 Arlington, VA 22203	AFRL/AFOSR RTA1	AFRL-AFOSR-VA-TR-2024-0064

12. DISTRIBUTION/AVAILABILITY STATEMENT
A Distribution Unlimited: PB Public Release

13. SUPPLEMENTARY NOTES

14. ABSTRACT
The information presented shows the characteristics of anisotropic porous materials (APMs). Both experimental and computation work is summarized. The design and fabrication of APM lattices for experiments are discussed, with the porosity varied in each direction to be low (~0.15), medium (~0.5), or high (~0.85) porosities. Both anisotropic and isotropic geometries are examined. The Darcy-Forchheimer model is used for data analysis with experiments conducted in uniform and fully developed flow conditions, with the best agreement of the model is seen for data acquired for high porosities. Experimental data are compared to DNS work, showing good agreement for anisotropic designs. In terms of computation work, a framework to characterize parameters of the DF law is introduced while quantifying the DF law performance in the highly nonlinear regime for equilibrium 2D flows. The implementation of DF within the ViCar3D solver and validation against existing literature for a direct numerical simulation (DNS) of a periodic turbulent channel flow is discussed, which shows a good agreement with existing work. Computational analysis of the performance of the DF law for a high-Re 2D separation bubble flow and the effects of porous substrate on the bluff body wake is introduced. Current work on experimental analysis of turbulent separation bubble control is briefly discussed.

15. SUBJECT TERMS

16. SECURITY CLASSIFICATION OF:			17. LIMITATION OF ABSTRACT	18. NUMBER OF PAGES
a. REPORT	b. ABSTRACT	c. THIS PAGE		
U	U	U	UU	10

19a. NAME OF RESPONSIBLE PERSON	19b. PHONE NUMBER *(Include area code)*
GREGG ABATE	425-1779

Standard Form 298 (Rev.5/2020)
Prescribed by ANSI Std. Z39.18

2021-2023 Final Technical Report

Passive Control of Non-Canonical Flows with Anisotropic Porous Materials

Award Number: FA9550-21-1-0286

F. Alvi & L. Cattafesta (FSU), Rajat Mittal & Charles Meneveau (JHU)

Students, Post-Docs and Research Faculty

- FSU – Sasindu Pinto (current Ph.D. student)
- JHU - Mostafa Aghaeijouybari (postdoctoral fellow)
- FSU – Yang Zhang (research faculty)
- JHU – Jung-Hee Seo (research faculty)

Abstract

The information presented shows the characteristics of anisotropic porous materials (APMs). Both experimental and computation work is summarized. The design and fabrication of APM lattices for experiments are discussed, with the porosity varied in each direction to be low (~0.15), medium (~0.5), or high (~0.85) porosities. Both anisotropic and isotropic geometries are examined. The Darcy-Forchheimer model is used for data analysis with experiments conducted in uniform and fully developed flow conditions, with the best agreement of the model is seen for data acquired for high porosities. Experimental data are compared to DNS work, showing good agreement for anisotropic designs. In terms of computation work, a framework to characterize parameters of the DF law is introduced while quantifying the DF law performance in the highly nonlinear regime for equilibrium 2D flows. The implementation of DF within the ViCar3D solver and validation against existing literature for a direct numerical simulation (DNS) of a periodic turbulent channel flow is discussed, which shows a good agreement with existing work. Computational analysis of the performance of the DF law for a high-Re 2D separation bubble flow and the effects of porous substrate on the bluff body wake is introduced. Current work on experimental analysis of turbulent separation bubble control is briefly discussed.

Background

In general, passive control using porous materials is more effective with materials with high permeability, but this requirement often conflicts in most engineering applications, with the need for high structural strength. However, in recent years, advances in materials, as well as fabrication/assembly of meta materials is driving the emergence of porous materials that have high permeability as well as high structural strength, and this is opening new opportunities for passive flow control. For instance, Pelacci (2021) proposed 3D woven-lattice periodic structures with high permeability and high specific stiffness for turbulence control and drag reduction of flow over bluff bodies. The hydrodynamic drag was reduced by up to 45% depending on the angular position of the porous insert on the cylinder substrate. Such high permeability materials allow interstitial flows with high Reynolds numbers, which are often far outside the range envisioned for the Darcy-Forchheimer law.

Main Research Objectives

- Use experiments and computational modeling to examine the characteristics of flows over high-porosity **APM** surfaces, with a focus on following turbulent flows
    - Zero and adverse pressure gradient turbulent boundary layers (TBLs)
    - Turbulent separation bubble (TSB)
    - Turbulent flow over a surface mounted obstacle (SMO)

Objectives achieved in the reporting period

Experimental -

- Design and fabrication of isotropic porous cubic lattice structures
- Characterization experiments under uniform flow conditions
- Design and fabrication of cylindrical porous structures
    - Tuft flow visualization on select specimen for refraction analysis
- Analysis of the effects of APM substrates on pressure gradient induced TSB using Stereoscopic Particle Image Velocimetry (SPIV)

Computational Modeling –

- Establish a framework to characterize parameters of the DF law, quantifying the DF law performance in the highly nonlinear regime for equilibrium 2D flows
- Implement DF within the ViCar3D solver and validate against existing literature for a direct numerical simulation (DNS) of a periodic turbulent channel flow
- Examine performance of the DF law for a high-Re 2D separation bubble flow
- Computational investigate effects of porous substrate on the bluff body wake

Accomplishments

Experimental 21-22

- Design and fabrication of isotropic porous material:- x_1 projected porosity ϵ_1 of the APM design method is repeated in all three directions to create isotropic designs. Void porosity ϵ is only a function of ϵ_1 (Figure 1). 3 designs with each design having high, medium and low nominal porosities of 0.85, 0.50 and 0.15 in all directions of a given design are created. Experiments were performed on these designs as discussed below.

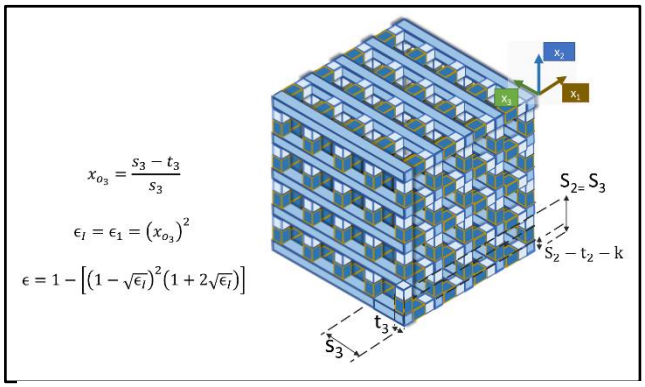

Figure 1: APM design and governing equations

- Characterization experiments under uniform flow conditions:- The 1-D square duct is removed from the experimental setup and the specimens are attached at the end of the contraction. Both anisotropic and isotropic mediums undergo experiments in a range of Re upto a Re = 2.166 x 10^3. Repeatability of data were verified by gathering multiple data samples for a given porosity, at different orientations (figure 2). Data were analyzed using the Darcy-Forchheimer model using spatially averaged velocity through cell openings and hydraulic diameter of cell openings as characteristic parameters (example shown for a design with $\epsilon_i = 0.500$ in figure 3). Linear least-square method with trust region optimization and Bi-square weighting robustness was used to create fit plots, with no zero offset.

Figure 2: Isotropic Porous Material Design

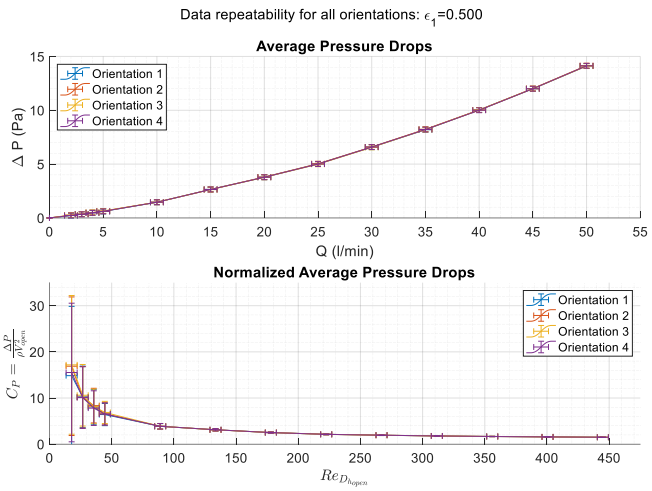

Figure 3: Experiment repeatability analysis a $\epsilon_i = 0.500$ design

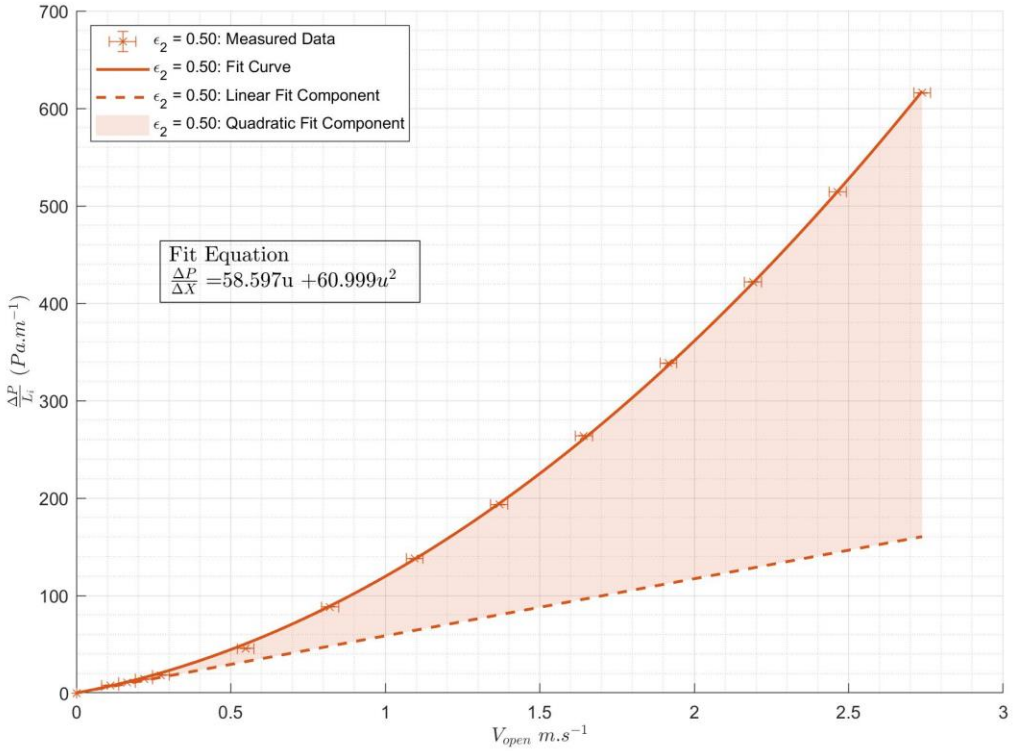

Figure 4: Darcy Forchheimer fit for a $\epsilon_i = 0.500$ data set

Notice that the linear region is very small and data from $V_{Open} \approx 0.2ms^{-1}$ are dominated by inertial effects. The first and second term in the RHS of the fit equation is used to determine

linear and inertial permeability respectively. Darcy-Forchheimer model was nondimensional using density, characteristic hydraulic diameter and velocity values. Data for high, medium and low nominal porosities across all 6 designs were plotted using the nondimensional Darcy-Forchheimer equation (figure 4). Linear least-square method with trust region optimization

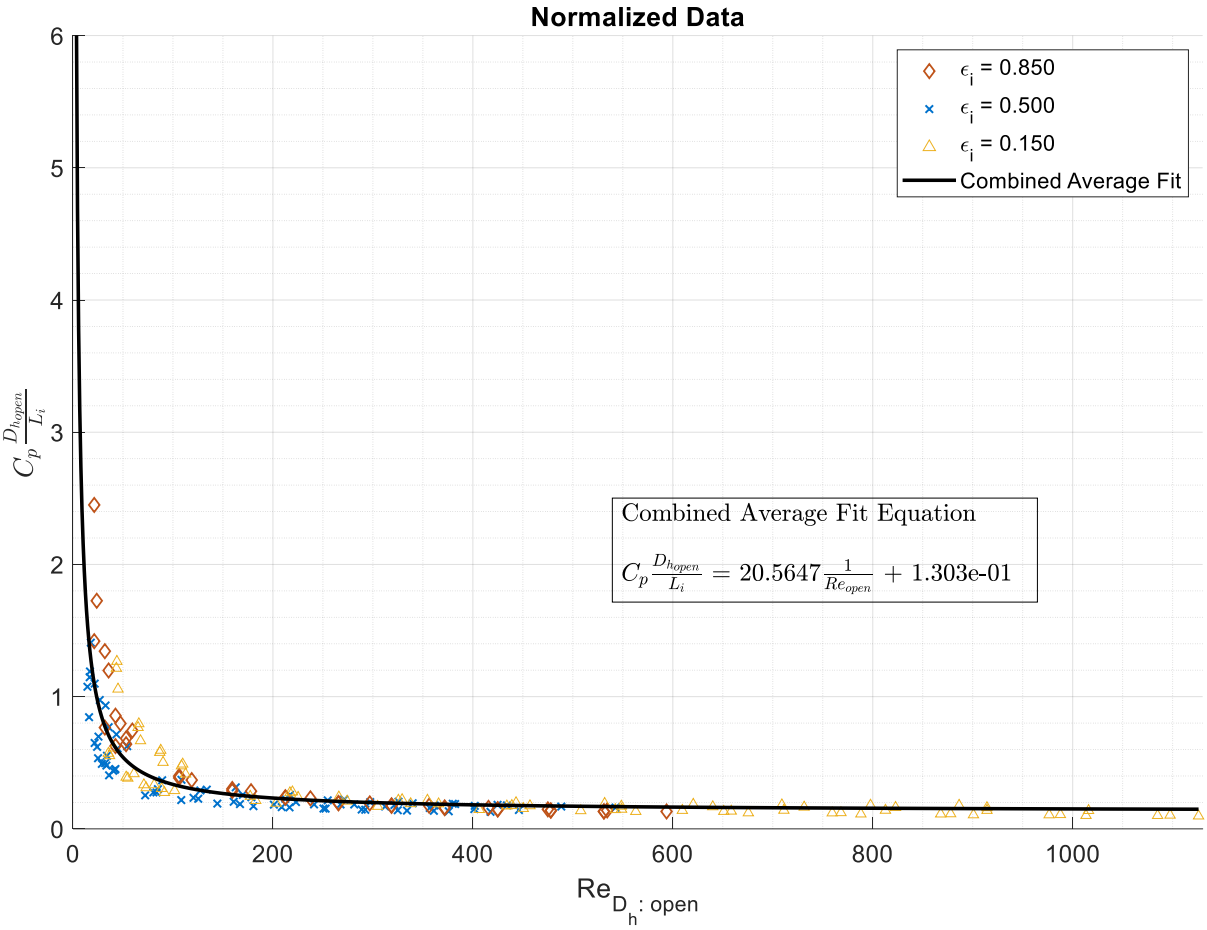

Figure 5: Normalized Darcy-Forcheimer data fit for high, medium and low porosities

was used for normalized fit plots as well, however no weighting function was applied as data come from different designs. A good convergence is seen for data sets for a given porosity, especially at higher Reynolds numbers. An acceptable convergence is seen across porosities as well. Similar to above discussion, nondimensional linear and inertial permeability are calculated using the first and second terms of the RHS of the fit equation. Permeability values, both dimensional and non-dimensionalized, calculated using fit plots for Darcy-Forchheimer are included in tables 1 and 2.

Table 1: Permeability Values

Porosity	Linear Permeability (K) [m^2]	Inertial Permeability (K_1) [m]
0.85	~8.6×10^{-7}	~8.4×10^{-2}
0.50	~3.1×10^{-7}	~2.0×10^{-2}
0.15	~4.2×10^{-7}	~1.1×10^{-2}

Table 1: Non-dimensional Permeability Values

Porosity	Non-dimensional Linear Permeability ($\widetilde{K}$)	Non-dimensional Inertial Permeability ($\widetilde{K_1}$)
0.85	2.97×10^{-2}	13.4
0.50	8.51×10^{-2}	7.09
0.15	6.83×10^{-2}	7.88

As mentioned in previous discussion, since inertial effects are dominating the flow, inertial permeability is the best parameter for analyzing porosities. For both dimensional and nondimensional values, inertial permeability is proportional to the porosity. However, normalized inertial permeability for 0.50 is lower than that of 0.15 porosity.

Experimental 22-23

The exact point when inertial effects are larger than viscous effects depend on the porosity of the design. Experimental data are analyzed for various designs with high ($\sim$ 0.85), medium ($\sim$ 0.50), and low ($\sim$ 0.15) projected area porosities and compared with select Direct Numerical Simulation (DNS) data. A zonal weighting approach with consideration to flow region variation through porous lattices was considered, which yielded the minimum error in convergence when analysis is similar to the projected flow blockage initially used. Dimensionless data analysis for anisotropic cases yielded a good convergence for high porosities. Convergence weakened with decreasing porosity. Comparison between similar-porosity isotropic and anisotropic cases yielded higher pressure losses for isotropic cases. It was concluded that the current scaling law is good for high porosities but not suitable across a range of porosities. For compared anisotropic cases, experimental data are in good agreement with DNS data, while a deviation is seen between experimental and numerical data for isotropic cases. Preliminary stereo PIV analysis of TSB flow with APM substrates showed that the average seperation bubble vanishes when APM substrates are attached.

Computational Modeling: 21-22

- The first set of simulations are performed for a 2D full periodic pressure-driven equilibrium regime. The simulations were performed for 14 values of Reynolds number: $Re = \{1, 5, 10, 20, 40, 60, 80, 100, 140, 180, 250, 400, 750, 1000\}$ and 5 values of $\alpha = \{0, 15, 30, 45, 60, 75, 90\}$. **Error! Reference source not found.** shows the c ontours of vorticity for the periodic aligned square-inclusions porous medium. Figure 6 shows the bulk velocity $\boldsymbol{u}_B$ in polar coordinates for different simulations. As the figure shows, at low Re, $\boldsymbol{u}_B$ complies with the direction of $-\boldsymbol{\nabla} P$. In high Re, however, $\boldsymbol{u}_B$ does not complies with the direction of $-\boldsymbol{\nabla} P$, and there appear to be specific directions that the flow is stable, a major consequence of dominating nonlinear effects due to emergence of vortex shedding in high Re. These directions happen to be aligned with x and y directions, where the sheltering effects from inclusions are maximum (requiring minimum drag).

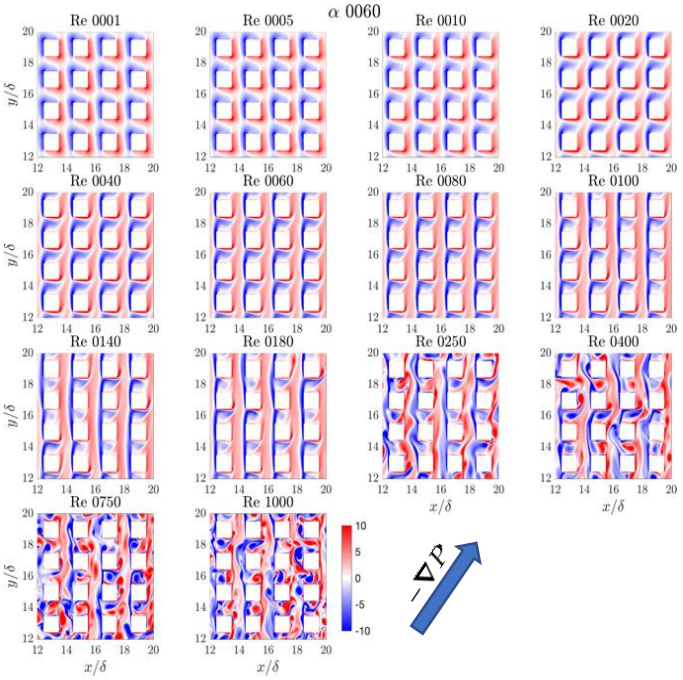

Figure 5 Contour of vorticity at $\alpha = 60$. Periodic aligned square-inclusion porous medium. Inclusions' length scale a=1. Domain lengths L_x=L_y=32. Porosity ϵ=0.75

- The 2D DF law reads as:

$$-\frac{\partial p}{\partial x} = \mu[K^{-1}]_{ij} u_j + [K_1^{-1}]_{ij} \rho |u| u_j \qquad (1)$$

The Darcy and Forchheimer tensors $\boldsymbol{K}$ and $\boldsymbol{K}_1$were predicted using the simulations data and employing the least-square-error method. The predicted values are

$\boldsymbol{K} = \begin{bmatrix} 6.70 & -0.01 \\ -0.01 & 6.70 \end{bmatrix} \times 10^{-2}$ and

$\boldsymbol{K}_1 = \begin{bmatrix} 7.83 & -5.90 \\ -5.90 & 8.57 \end{bmatrix}$.

The prediction accuracy is tested in Figure for the bulk velocity vectors (given the pressure gradient), and the results are compared with the true vectors. As the figure shows, the DF law performs well in low Re regime, however its performance reduces significantly for the high Re one. This shows that the original DF law does not capture the nonlinear effects dominated in high Re flows, demanding for an alternative approach/formulation.

- The DF model is then implemented into ViCar3D solver, and the results were validated against those of Samanta et. al. (JFM, 2015, vol 784, pp 681-693) for a DNS of periodic channel flow over a porous medium. The simulation setup and the mean and turbulence profiles are shown in 8 (a-

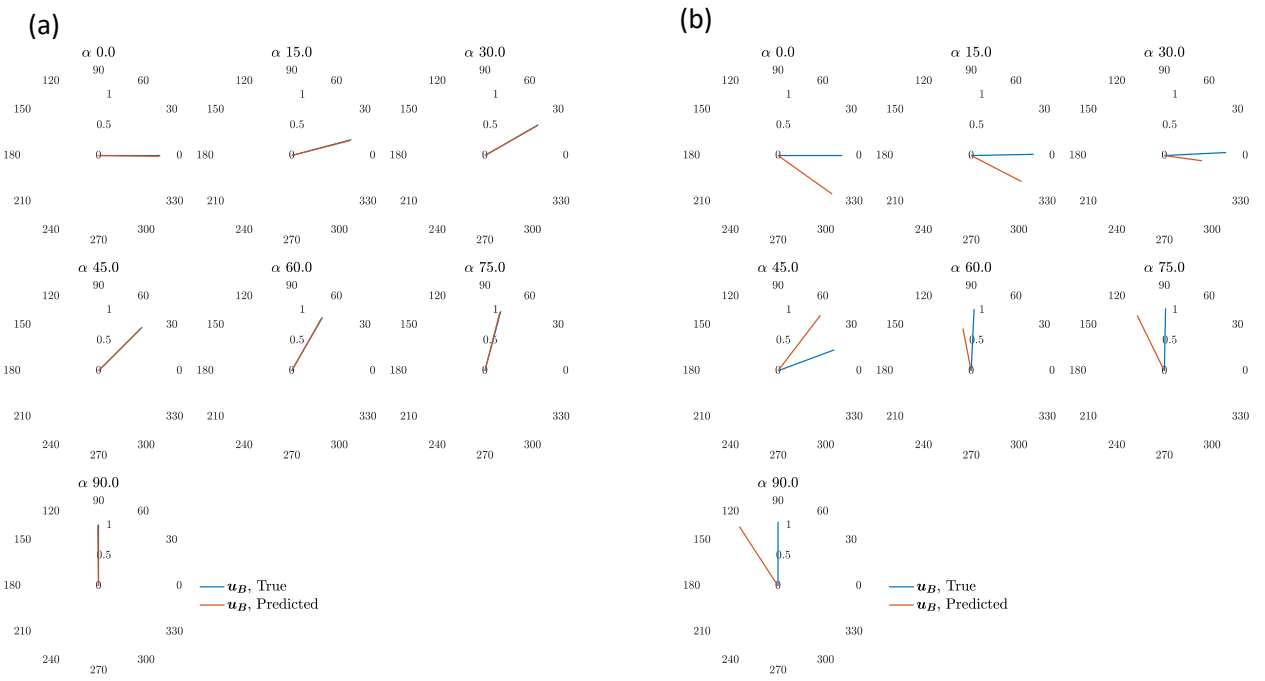

Figure 7 Testing DF law using the predicted $\boldsymbol{K}$ and $\boldsymbol{K_1}$at low Re (a) and high Re (b).

c), respectively, indicating that the results of the implemented DF model are in good agreements with the results of Samanta et. al.

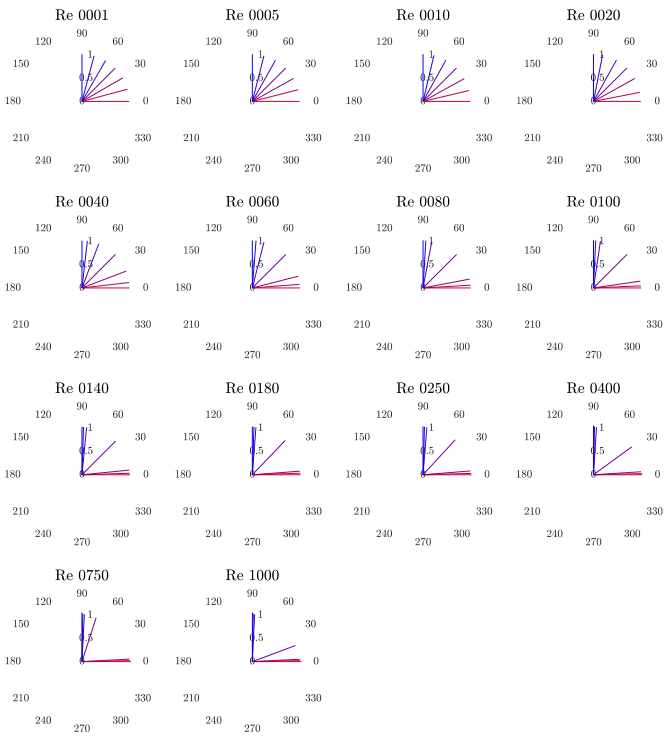

Figure 6 Bulk velocity in polar coordinate. Lines from $\alpha = 0$ (in red) to $\alpha = 90$ (in blue).

- A 2D boundary layer flow over the aligned square-inclusions porous medium with separation bubble is simulated by both capturing the inclusions using an IB method and modeling them using the DF law. The results (mean velocities and fluctuation kinetic energy FKE) are shown in Figure . Although the results of mean profiles match between the two simulations, there are subtle differences in the FKE profiles, the sources of which are attributed to the nonlinear effects at the Reynolds number of the simulations.

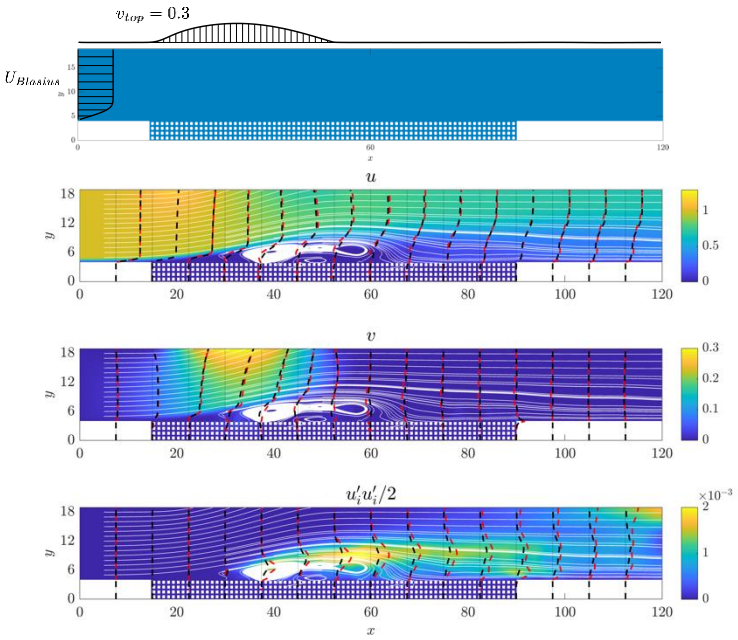

Figure 9 Separation bubble over aligned square-inclusions porous medium. Inclusions are captured using an IBM (red dash lines and the contour plots) and modeled using the DF law (black dash lines). Re=500 and $\epsilon = 0.75$.

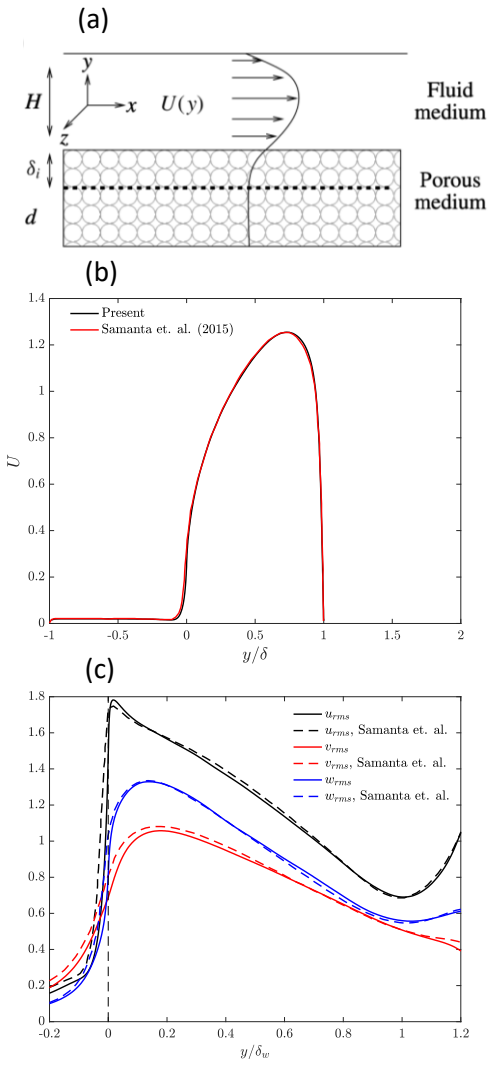

Figure 8 Implementation and validation of the DF model within ViCar3D solver.

- Flow over a wall mounted rib is simulated to investigate the effects of porous substrate on the flow separation in the wake of bluff body. The simulations are performed by the DF law implemented on the ViCar3D immersed boundary solver.
- In the first set of simulations, the wall under the square rib (size h) is replaced with a porous substrate of thickness 2h. Two different permeabilities (0.02 and 0.087 mm^2) are considered. The solid wall case is also simulated for the comparison.
- The simulation results show that the unsteady flow separation observed in the solid wall case diminishes with the porous substrate especially for the higher permeability (see Figure). The results agree with the experimental results of Suga et al.(Flow Turbulence Combust, 2013).

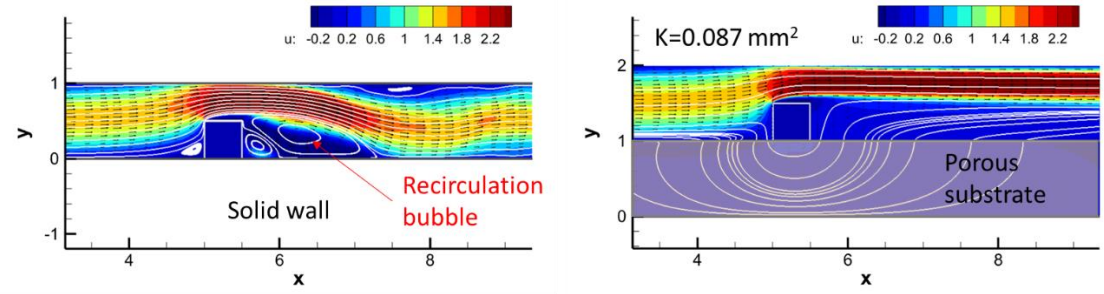

Figure 10 Flow over a wall mounted square rib. Left: Solid wall, Right: Porous substrate, porosity of 0.8 and permeability of 0.087 mm^2.

- The identified mechanism is that the momentum redirected through the porous substrate fills out the separating region behind the bluff body.
- To find the optimal size of the porous substrate, additional simulations are performed for the various width and depth of the porous substrate under the rib. Based on the simulation results, it is found that a small and thin substrate (width of 1.4h and depth of 0.2h) effectively diminishes the unsteady flow separation in the wake of the bluff body (Figure).

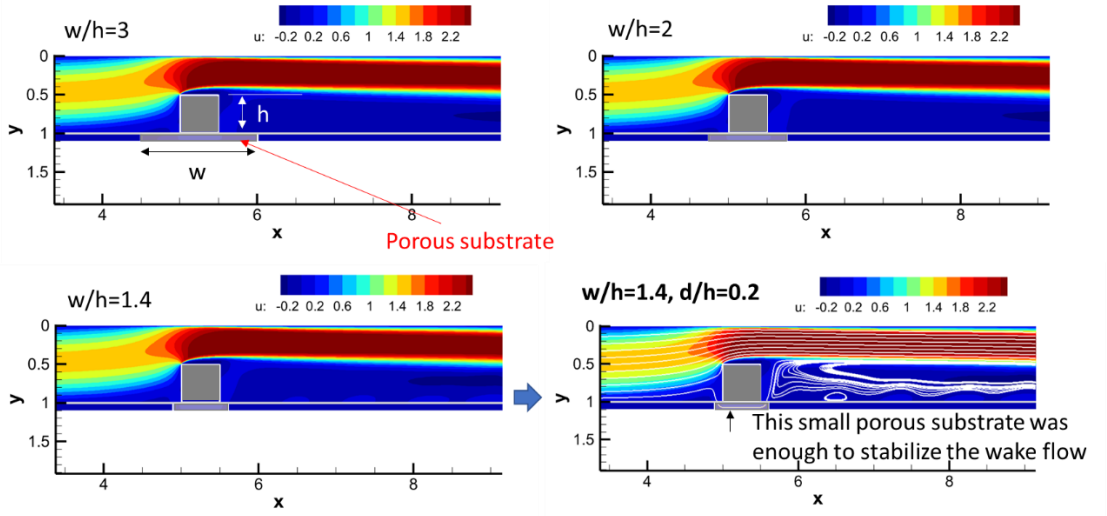

Figure 11 Simulation results for various porous substrate size. w: width of the substrate, d: depth of the substrate, h: size of the solid rib over the substrate.

Computational Modeling: 22-23

Through DNS, we examine the predictive accuracy of the standard Darcy-Forchheimer (DF) law, which is often used to model porous media flows, for inclusion Reynolds numbers (Re) ranging from the low, linear regime to the high nonlinear regime where unsteady effects such as vortex shedding become evident. We consider two different inclusion shapes - square and circular - and three different arrangements of the inclusions - inline, staggered and random. The numerical simulations show that the DF law performs well for low-Re flows, irrespective of the inclusion configuration. For intermediate/high-Re flows, the DF law is adequate only when the arrangement is highly random.

However, for the regularly arranged topologies or less random geometries at intermediate/high-Re flows, the DF law performance diminishes significantly due to flow sheltering and redirection (``flow refraction'') effects that arise from flow separation and vortex shedding in the wake of the inclusions. It is shown that the standard DF law, in which the nonlinear permeability tensor is independent of orientation, does not capture such effects. We generalized the DF law to capture flow redirection effects by allowing the Forchheimer permeability tensor to depend on the flow orientation with respect to the principle geometrical directions of the porous geometry, and examine this generalized DF law for these flows.

Future Work

Further analysis of cylindrical models, including anisotropic porosity designs will be conducted. Schlieren imaging will be conducted to capture refraction for select models of cylindrical APM designs. Further PIV, SPIV (and possibly PTV) experiments will be conducted on turbulent separation bubble flow with APM substrates attached. Simulations of turbulent separation bubble over APM will be conducted for different porous media geometries. The effects of porous media on mean and turbulence fields will be examined, accompanied by Dynamic Mode Decomposition analysis.

Publications

- “Characterization of Periodic Lattice Anisotropic Porous Materials for Passive Flow Control”, AIAA AVIATION Forum, Jun. 2023, doi: 10.2514/6.2023-3448
- “Passive Control of Non-Canonical Flows with Anisotropic Porous Materials”, APS Division of Fluid Dynamics 75th Annual Meeting, Nov 2022.
- “Darcy-Forchheimer law for porous media flows in the highly-nonlinear regime for passive flow control”, APS Division of Fluid Dynamics 75th Annual Meeting, Indianapolis IN, Nov 2022.
- “Control of wall-mounted bluff body wake by a porous substrate”, APS Division of Fluid Dynamics 75th Annual Meeting, Indianapolis IN, Nov 2022.
- “Effect of Interstitial Vortex Shedding on Darcy-Forchheimer Law Predictions in High-Re Porous Media Flows”, Direct in-Person Colloquium on Vortex Dominated Flows, Breckenridge, CO, May 2023.
- “Generalized Darcy-Forchheimer law including directional effects”. Submitted to the Journal of Fluid Mechanics.